Pharmacogn. Mag.
A multifaceted peer reviewed journal in the field of Pharmacognosy and Natural Products
www.phcog.com | www.phcog.net

ORIGINAL ARTICLE

Herniarin, a Natural Coumarin Loaded Novel Targeted Plasmonic Silver Nanoparticles for Light Activated Chemo-Photothermal Therapy in Preclinical Model of Breast Cancer

Pritha Bose[1], Shakti P Pattanayak[1,2], Amiya Priyam[3]

[1]Department of Pharmaceutical Sciences and Technology, Birla Institute of Technology, Mesra, Ranchi 835215, Jharkhand, [2]Department of Pharmacy, School of Health Sciences, Central University of South Bihar (CUSB), Government of India, [3]Department of Chemistry, School of Physical and Chemical Sciences, Central University of South Bihar, Gaya, India

Submitted: 29-May-2020 Revised: 15-Jun-2020 Accepted: 11-Aug-2020 Published: 30-Nov-2020

ABSTRACT

Background: The conventional chemotherapeutic approach for breast cancer involves use of free drug substances that succumb into considerable systemic toxicity. For the past few decades biologically active phytochemicals like coumarins have gained much interest against breast cancer. However, there are lacunas in direct use of these potent biomolecules that impede their pharmacological functions. On the other hand, recent years have also witnessed great advancements in stimuli actuated nanotherapeutics as combined treatment strategies in critical breast cancer cases. **Objectives:** In this study we formulated novel pentagonal plasmonic silver nanoparticles as folate receptor targeted light responsive nano-delivery platform for a potent coumarin derivative, Herniarin to improve its therapeutic proficiency. **Materials and Methods:** Primarily, we synthesized plasmonic silver based nanoscopic carrier for herniarin to facilitate its tumor targeted delivery via folate receptors. These formulated nanoparticles (Herniarin quenched, folic acid furnished, HER-FA-AgNPs) were subjected to series of physicochemical tests, followed by detailed *in-vitro* and *in-vivo* testing in breast cancer cell lines and DMBA induced breast cancer model in rats, respectively. **Results:** The pentagonal nanoparticles observed in transmission electron microscopy demonstrated strong plasmonic tunability in the NIR region while its key feature of transforming light into heat energy when exposed to laser (800 nm) allowed photothermal therapy to supplement the chemotherapeutic potential of Herniarin as illustrated in various *in-vitro* studies. The *in-vivo* studies including detailed cellular investigations of breast tissues through Field Emission Scanning Electron Microscope and histopathology reflected the improved outcome of combined therapeutic modalities (hyperthermia + chemotherapy) achieved by HER-FA-AgNPs. **Conclusion:** Thus, these novel nanoparticles may serve as an efficient as well as safe drug-disposing vehicle for combined and strategic therapy of breast cancer.

Key words: Breast cancer, DMBA, herniarin, hyperthermia, photothermal therapy, plasmonic silver nanoparticles

SUMMARY

- We followed citrate hydrazine method for synthesizing plasmonic silver nanoparticles by carefully modulating the hydrogen bonding for breast tumor tissue specific delivery of HER. The combined chemo-photothermal efficacy of these HER-FA-AgNPs were evident in all the *in-vitro* and *in-vivo* studies performed for the current studies.

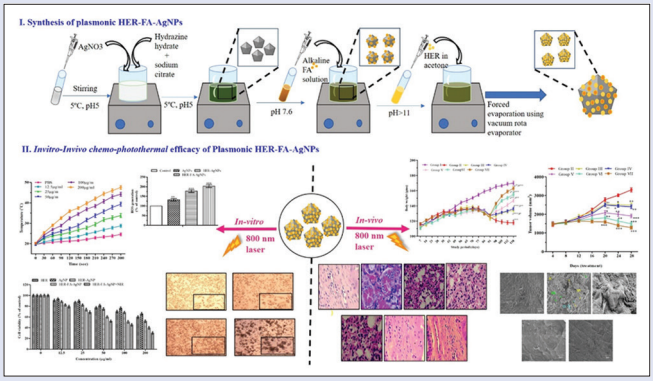

Abbreviations used: HER: Herniarin; HER-FA-AgNPs: Herniarin quenched folate receptor targeted silver nanoparticles; c.w. NIR laser: Continuous wavelength near-infrared laser; MTT: 3-(4,5-dimethylthiazol-2-yl)-2,5-diphenyl tetrazolium bromide; ROS: Reactive oxygen species; FESEM: Field Emission Scanning Electron Microscope; TNBC: Triple negative breast cancer.

Correspondence:

Dr. Shakti P Pattanayak,
Department of Pharmaceutical Sciences & Technology, Birla Institute of Technology, Mesra, Ranchi 835215, Jharkhand.
Department of Pharmacy, School of Health Sciences, Central University of South Bihar (CUSB), Govt. of India, Gaya-824209, India.
E-mail: sppattanayak@cusb.ac.in; sppattanayak@bitmesra.ac.in

DOI: 10.4103/pm.pm_223_20

Access this article online
Website: www.phcog.com
Quick Response Code:

INTRODUCTION

Breast cancer is declared as a global public health dilemma accounting for an estimated 20,08,8849 (11.6%) new cancer cases worldwide. For the past 2 decades this life-threatening malignancy is the foremost cause of mortality in women population all over the globe. Despite current advancement in surgery, chemotherapy and even radiotherapy, breast cancer patients often suffer from chances of recurrence and metastasis to distant organs. Also, among various subtypes, triple negative breast cancer (TNBC) patients face the worst prognosis.[1] These challenges related with conventional chemotherapy thus have oriented the attention

Cite this article as: Bose P, Pattanayak SP, Priyam A. Herniarin, a natural coumarin loaded novel targeted plasmonic silver nanoparticles for light activated chemo-photothermal therapy in preclinical model of breast cancer. Phcog Mag 2020;16:S474-85.

of researchers towards combined therapeutic strategies that will not only surpass the limitations of single modality but also prevent healthy tissue damage. As a consequence of significant evolution of the phytochemical research, diversified natural compounds have been identified to have therapeutic efficacy with reduced side effects, which are also capable of minimizing the dose of conventional drugs.[2,3] Natural coumarin derivatives possess anti-tumor,[4] antioxidant,[5] anti-inflammatory,[6] antiviral and other different pharmacological properties. Herniarin (HER), a novel 7-methoxycoumarin derivative, naturally occurring in *Ruta graveolens* L., *Citrus sinensis*, *Hordeum vulgarae*, *Matricaria chamomilla* L., *Lavandula angustifolia, Tagetes lucida* flowers etc., which possesses evident cytotoxic potential against MCF7[7] and laryngeal cancer cell lines[8] has recently been reported to have significant *in-vivo* anti-breast cancer potential.[9]

However, hydrophobicity, poor stability, along with high rate of tissue/plasma metabolism and elimination results in primary challenges towards the efficacy of these biomolecules by limiting bioavailability at targeted tumor site.[10] Active tumor targeting by silver Nano carriers play a major role in circumventing these obstacles. Folic acid (FA, tumor specific molecule) functionalized silver nanoparticles (AgNPs) thus selectively target cancer cells by recognizing its counterpart, the folate receptors (FRs) that are majorly overexpressed in breast cancer cells and render superior biocompatibility of the formulated nanoparticles.[11]

With promising advancement in the nanotechnology field, AgNPs have received much attention in biomedical research specially in cancer theranostics.[12] On the other hand, the AgNPs also serve as an encouraging nano-delivery system for various drugs that confers in accretions of breast cancer treatment strategies. Intracellular released silver ions by the AgNPs are known to produce reactive oxygen species (ROS) that mediate mitochondria dependent intrinsic apoptosis.[13,14] The plasmonic silver nanoparticles owing to their robust plasmon tunability in the ultraviolet (UV)-Vis-NIR region escalates the efficiency in cancer treatment as light to heat converters inducing photothermal therapy (PTT).[15] These nanoparticles after resonating with NIR laser (of specific wavelength) in the biological transparent window (750–1200) nm accentuate hyperthermia (41–44)ºC in tumors followed by localized irreversible detrition of cancer tissue.[16,17] PTT is currently being envisaged as an archetypal anticancer therapy option favored by its facile, manageable and biosafety features.[18,19]

Till date no study has reported silver nano-formulations encapsulating HER for breast cancer therapy. Thus, fundamental focus of the current study was to optimize and evaluate anisotropic plasmon tunable silver nanocargos for HER to bolster an attractive tumor-targeted, light activated hyperthermia mediated chemotherapeutic platform for breast cancer through *in-vitro* and *in-vivo* analysis.

MATERIALS AND METHODS

Materials

Silver nitrate (99.5%, 209139-25 g), trisodium citrate (99% S1804-500 gm), hydrazine hydrate (80%, 10217-52-4), sodium hydroxide (98%, D3254-100 mg) and HER (W515809) were procured from Sigma-Aldrich (St. Louis, MO, USA), while folic acid dihydrate (A14300-25 g) was purchased from Alfa Aesar (Heysham, England). Every reagent in this study was assured of high purity and of analytical grade.

Cell line and cell culture

The human breast cancer (MDA-MB-231) cell lines were procured from National Centre for Cell Science Pune, India and maintained in Dulbecco's modified eagle medium (DMEM)/F12 culture medium supplemented with 10% fetal bovine serum (FBS), streptomycin (100 U/mL) and penicillin (100 mg/mL) in a humidified atmosphere of 5% CO_2 at 37°C.

Synthesis of plasmonic anisotropic AgNPs

The synthesis of AgNPs were performed according to previously described method.[20] Briefly, initial mixing of $AgNO_3$ (1 mM, 10 ml) and citrate (80 mM, 0.5 ml) solution was subsequently followed by hydrazine hydrate (40 mM, 2 ml) addition to it with constant stirring, the overall pH being maintained at 5 until a green color appeared. The temperature of reaction mixture was maintained at 5°C throughout the procedure. For adjusting pH of the solution 1M NaOH or 1M H_2SO_4 was dropwise added.

Synthesis of folate receptor targeted AgNPs (FA-AgNPs)

FA conjugation with AgNPs was performed following a novel and simple method. FA solution (160 mM, 0.5 ml) was added to already synthesized AgNP solution (12.5 ml) (pH 7.6) under constant stirring and then the reaction mixture was allowed to rest for 2 h with subsequent concentrating it to at least 1/5th of the initial volume in vacuum desiccator. Following this, isopropyl alcohol (IPA, 10 ml) was added to the sample and then centrifuged (4500 rpm 10 min). The pellets thus obtained after decanting the resulting supernatant was again dissolved in IPA and subjected to centrifugation under similar conditions as previously stated. After 2nd washing, synthesized FA-AgNPs pellets were collected and lyophilized to powdered form for further use and characterization.

Synthesis of HER quenched folate receptor targeted AgNPs (HER-FA-AgNPs)

A one pot synthesis protocol for HER quenching to FA-AgNPs was followed. HER (80 mM) was primarily dissolved in acetone (30 ml) and the solution was added to synthesized FA-AgNP solution (pH adjusted to 10) with mild initial stirring. The reaction mixture was then allowed to rest until separation of the organic layer which was subsequently removed by rapid forced evaporation using rotary evaporator. After this, the resultant aqueous solution containing quenched drug molecules was adequately concentrated in vacuum desiccator and then centrifuged by adding IPA with successive washing (x2, IPA) to obtain final pellets of HER-FA-AgNPs. These pellets were then lyophilized, powdered and stored for further use. HER and folic acid used for the synthesis of HER-FA-AgNPs were in the ration of 1:2.

Drug loading content of HER-FA-AgNPs

HER loading efficacy of synthesized AgNPs was estimated by an indirect method. HER-FA-AgNP solution was centrifuged at 10,000 rpm for 30 min. Then drug concentration in the resultant supernatant was quantified by UV absorbance at 322 nm using UV – visible spectroscopy (UV-2450, Shimadzu, Kyoto, Japan) and the HER loading percentage in synthesized FA labelled AgNPs was calculated by the following formula.

Loading efficiency = $wo/w \times 100$

Where *wo* is the weight of HER loaded on FA-AgNPs and w is the weight of synthesized FA-AgNPs.

Characterization of HER-FA-AgNPs

UV-Vis-near-IR absorption spectroscopy was conducted after diluting the nanoparticle samples twice with Millipore water using UV-2450 (Shimadzu, Kyoto, Japan) spectrophotometer. The possible composition of synthesized nano-formulation was analysed using Fourier transform

infrared (FT-IR) spectroscopy (IR-Prestige 21; Shimadzu Corpn., Japan) in scanning wave number ranging from 400 to 4000 cm^{-1} at 2 cm^{-1} resolution according to KBr pellet method while X-ray diffraction (XRD) was performed for determining the nature of synthesized NPs (Rigaku, Japan). Transmission electron microscopy (TEM, FEI-Tecnai G2 20 S-TWIN) was carried out for establishing the morphological features (size, shape as well as structure) of anisotropic nanoparticles along with energy dispersive X-ray (EDAX) and selected area electron diffraction (SAED) analysis. For TEM experiment few drops of synthesized nanoparticles on copper grids (carbon coated) (Ted Pella, product code: 01800) were dried immediately in vacuum desiccator. A Zeiss microscope (operating voltage; 200 kV) was used for imaging while SAED helped in revalidation of crystallinity. Also, dynamic light scattering (DLS) was performed for determining average size distribution of NPs, polydispersity index and zeta potential (surface charge) in Nano ZS Zetasizer (Malvern Instruments Ltd., Malvern, UK) following appropriate dilution of the samples.

To check stability, HER-FA-AgNPs were incubated in 3 biologically significant medium such as deionized water, cell culture medium (DMEM, glucose and 10% FBS) and phosphate buffer (PBS), respectively, followed by regular analysis of hydrodynamic diameter and PDI (Nano ZS Zetasizer; Malvern Instruments Ltd., Malvern, UK) of the NPs for a period of 14 days.

Estimation of *in-vitro* HER release from HER-FA-AgNPs

The release pattern of HER from synthesized nanoparticles was determined using the dialysis method at 37°C in respective pH of 7.4 and 5.5 corresponding to physiological systemic environment. Briefly, suspension of HER-FA-AgNP (containing drug equivalent 5 mg) in PBS (1 ml) was placed in dialysis bag (MW CO 2000 Da; Sigma Aldrich). Before submerging the dialysis bag in 10 ml PBS, the pH was adjusted to 7.4 and 5.5, respectively, and then were incubated at 37°C in a water bath with constant stirring (130 rpm), respectively. At regular and predetermined time intervals, withdrawal of 1 ml of PBS containing leached drug was immediately followed by replacement with equivalent amount of fresh PBS maintained at similar conditions. The withdrawn samples were analyzed using UV-2450 (Shimadzu, Kyoto, Japan) spectrophotometer at 322 nm. The experiments were carried out in triplicates at individual selected pH.

Quantification of photothermal efficiency of HER-FA-AgNPs

The photothermal efficiency of HER-FA-AgNPs was measured by exposing aqueous solution of various concentrations of HER-FA-AgNPs (12.5, 25, 50, 100 and 200 µg/ml) taken in quartz cuvette to NIR laser (800 nm, 1.5W/cm^2) for 5 min. The temperature variations of the solution were monitored every 30 s by using an online-type thermocouple thermometer. PBS used as control was also irradiated by NIR laser under same condition for 5 min.

In-vitro cytotoxicity assessment

MTT assay was carried out for determination of cytotoxicity.[21] Briefly, MDA-MB-231 (10^4 cells/well) cells were primarily seeded in 96 well plates and after 24 h, were incubated with varying concentrations of pure HER, AgNPs, HER-AgNPs HER-FA-AgNPs and HER-FA-AgNPs + NIR (800 nm, 1.5 Wcm^{-2},5 min) for specified period of time (up to 48 h). For each treatment schedule, six replicates were used. Following this, the cells were incubated for an additional 2 h with 0.5 mg/ml of MTT solution at 37°C. Then, after aspirating MTT contained medium was aspirated DMSO (200 µl) was introduced in each well to ensure solubilization of the resulting formazan product. The absorbance (Abs) was determined at 570 nm by a microplate reader and calculation for comparative inhibition was done following

$(Abs_{Control} - Abs_{treatment})/Abs_{Control} \times 100\%$.

In-vitro photothermal therapy analysis

Phase (light) contrast microscopy was used to deduce the proficiency of HER-FA-AgNPs to accomplish hyperthermia under laser irradiation characterized by cellular degeneration and altered morphological features of MDA-MB-231 after subsequent treatment with[22] with PBS, PBS + NIR (800 nm, 1.5 Wcm^{-2}, 5 min), HER-FA-AgNPs and HER-FA-AgNPs + NIR (800 nm, 1.5 Wcm^{-2}, 5 min). Leica DME and canon camera were employed to capture the photos.

Intracellular reactive oxygen species levels

Quantification of ROS production[23] was performed by dichlorodihydroflurescin diacetate (DCFH-DA) analysis kit as per manufacturer's protocol. Briefly, seeding of MDA-MB-231 cells was antecedent to treatment of cells with required concentrations AgNPs, HER-AgNPs and HER-FA-AgNPs. Then the medium was removed and cells were further incubated (37°C) for 30 min with DCFH-DA (10 µM) and Hanks buffered salt solution (HBBS, 100 µl). Measurement of ROS was performed with spectrofluorometer.

Experimental animals and study design

Virgin female Sprague-Dawley (SD) rats (50–55 days old) necessary for the study were obtained from Central Animal Facility, Birla Institute of Technology (BIT) Mesra, Ranchi, Jharkhand, India (Reg. No. 1968/PO/Re/S/17/CPCSEA). The entire study protocol was executed in congruence with International standards of animal habitat, victuals with prior approval from Institutional Animals Ethics Committee, BIT Mesra, Ranchi, India) (1972/PH/BIT/61/18/IAEC).

Animals were randomly distributed such that each of 7 experimental groups had 6 rats, respectively. Group I (control) animals were devoid of any interventions except only vehicle (olive oil [0.5 ml] administration on the day of induction) (CDH, New Delhi, India). Group II rats were subjected to cancer induction by injecting uniformly suspended DMBA (20 mg in 0.5 mL olive oil) following slightly modified air pouch technique[24] and thus was designated as induced control group. Animals belonging to group III-VII were considered as treatment groups. Group III animals received tail vein injections of AgNPs (40 mg/kg, b.w.), group IV rats were administered with pure HER (20 mg/kg, b.w., i.v.) while group V and VI animals received HER-AgNPs and HER-FA-AgNPs (equivalent to amount of raw HER administered, i.v.). Group VII animals were subjected to irradiation with c.w. NIR laser (800 nm, 1.5 W/cm^2 for 5 min) 24 h post-HER-FA-AgNP administration (i.e., for 14 days, every alternate days of 28 days of treatment protocol). Treatment in all the groups was continued for 28 days following promotional stage (90 days) from administration of DMBA with weekly monitoring of body weight as well as tumor location by palpation. After completion of treatment protocol, animals were sacrificed by cervical dislocation and perfused with subsequent isolation of mammary tissues. Section of breast tumor were preserved in buffered formalin for histopathological and Field Emission Scanning Electron Microscope (FESEM) analysis.

Histopathological analysis

The isolated tumor and breast tissues preserved in buffered formalin were embedded in paraffin wax and fine sections (6–8 µm) of these paraffin blocks were cut using rotary microtome. Then, haematoxylin

and eosin dye staining technique was employed according to standard experimental protocol.[25]

Field Emission Scanning Electron Microscope analysis of breast tissues

The breast tissue extracted from different animals groups were subjected to initial fixation using 10%v/v of buffered formalin followed by sequential dehydration with ethanol of successive ascending strength (70% v/v for 3 h followed by 80%, 90%, 100% v/v of ethanol for a hour each).[25] Tissue sample drying with the help of critical point dryer preceded their stub mounting. Then they were exposed to sputter-coating with gold and subjected to viewing under FESEM (Sigma 300, ZEISS, Carl Zeiss).

Statistical analysis

Statistical comparisons of the data were determined by one-way ANOVA, followed by Bonferroni's multiple comparison tests with similar no. of sample size. The level of significance was measured at $P < 0.05$. All data were represented as mean ± standard error of the mean.

RESULTS

Ultraviolet-visible-near infra-red absorption spectra analysis of the synthesized AgNPs

Robust plasmon tunability in the visible (Vis)-NIR window was exhibited by the AgNPs synthesized using optimum concentration (40 mM) hydrazine at pH 5 and 5°C. As demonstrated in Figure 1a, 2 distinctive surface plasmon resonance (SPR) peaks were observed in the spectral analysis, the first (SPR1) at 410 nm, typical of silver NPs and SPR2 at 817 nm. After labelling the nanoparticles with FA along with HER quenching, the optically active HER-FA-AgNPs exhibited significant red shift of both the SPRs (SPR1: 410 nm→453 nm; SPR2: 800 nm→855 nm) [Figure 1b]. Although SPR1 became less prominent, SPR2 showed strong NIR individual resonance and the shift in SPRs indicated successful conjugation of FA and HER.[26] Moreover, the characteristic absorption peaks of HER (318 nm and 216 nm)[27] as well as that of FA (360 nm)[20] as observed in the spectral analysis of their physical mixture [Figure 1c] was also detected in the HER-FA-AgNPs spectrum [Figure 1b] but were slightly shifted to 322 nm, 220 nm and 364 nm, respectively, that represented successful binding of both HER and FA on the surface of AgNPs.

Fourier-Transform Infrared analysis

FT-IR analysis efficiently explores the surface conjugation of FA and HER. Figure 1d represents identifying peaks of raw FA, HER, their physical mixture (FA + HER (R)) along with respective nanoparticles FA-AgNPs and HER-FA-AgNPs. Raw HER showed characteristic peaks/bands 1732.01 cm^{-1} (corresponding to ketonic group), 1608.02 cm^{-1} (corresponding to C = C), 1534.44 cm^{-1} (correlating to aromatic structure), 1201.01 cm^{-1} and 1291.12 cm^{-1} (correlating to OMe). Also, prominent IR bands were visible at 817.33 cm^{-1}, 1012.77 cm^{-1}, 1163.23 cm^{-1}, 1380.62 cm^{-1} and 1438.02 cm^{-1}.[27] FA (raw) demonstrated peaks at 1109.74 cm^{-1} (typical of C-O alcoholic stretch of pteridine ring), 1688.22 cm^{-1} (due to C = O bond stretching vibration of carbonyl group),

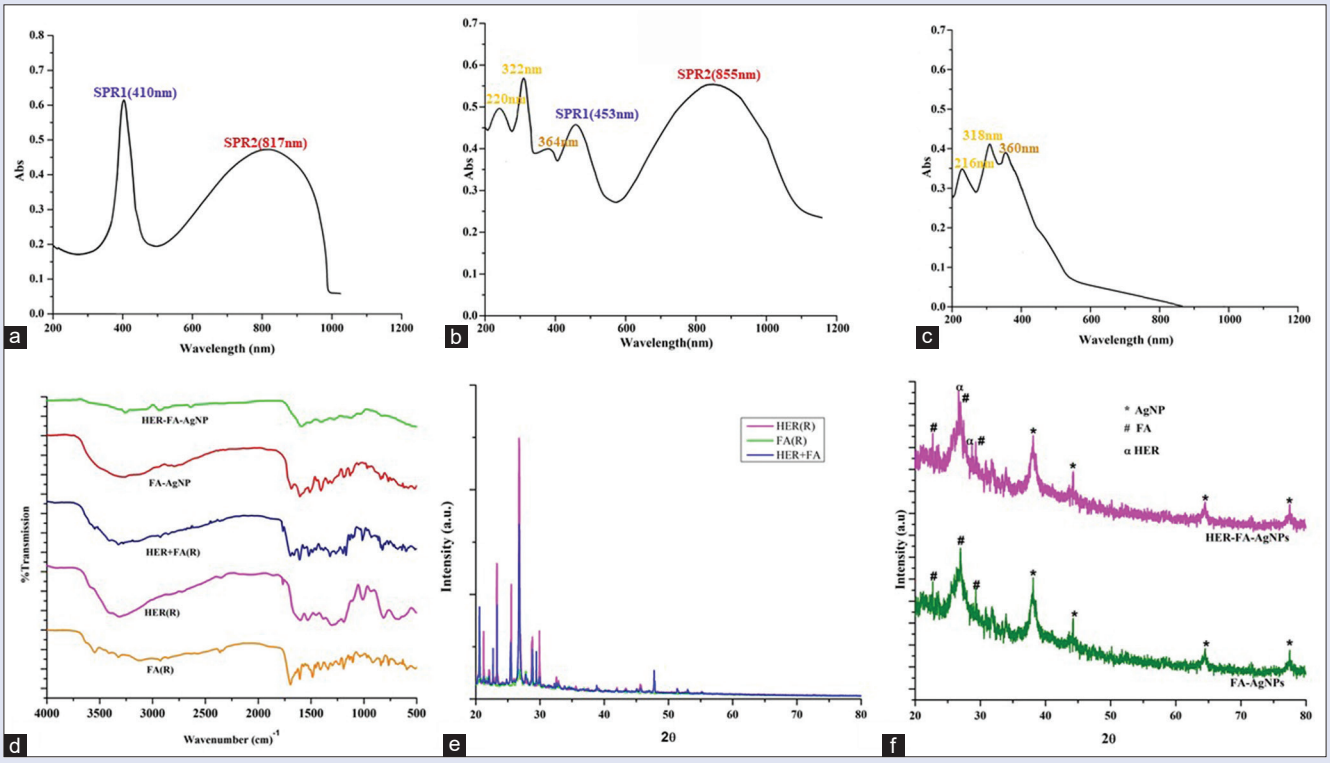

Figure 1: Synthesis and characterization of HER quenched FA modified plasmonic anisotropic silver nanoparticles (HER-FA-AgNPs) (a) plasmon peaks of AgNPs (SPR1: 410 nm and SPR2: 817 nm) formulated in single step chemical method, (b) characteristic absorption peak of HER at 220, 322 nm and FA at 364 nm with significant of red shift of SPR1 (453 nm) and SPR2 (855 nm) denoting successful drug quenching and folic acid conjugation, (c) characteristic absorption peaks of HER and FA in physical mixture, (d) Fourier transform infrared spectra showing characteristic IR bands or peaks of FA (r), HER (r), FA + HER (physical mixture) (r), FA-AgNPs and HER-FA-AgNPs, (ei and eii) X-ray diffraction spectral pattern showing characteristic peaks of FA (r), HER (r), FA + HER (physical mixture) (r), FA-AgNPs, HER-AgNPs and HER-FA-AgNPs; HER: Herniarin, FA: Folic acid, FA-AgNPs: Folic acid fabricated silver nanoparticles, HER-AgNPs: Herniarin quenched silver nanoparticles, HER-FA-AgNPs: Herniarin quenched folic acid modified silver nanoparticles, AgNPs: Silver nanoparticles

3126.17 cm^{-1} and 3319.30 cm^{-1} (corresponding stretching vibration of N-H and O-H groups).[20] The IR spectral analysis of physical mixture of HER and FA also revealed the presence of all the peaks typical of HER and FA with minor shift or broadening. Although the peaks corroborating to raw HER and also FA appeared in the IR spectrogram of different synthesized AgNPs, there were certain changes in the IR spectral pattern and alterations in these vibrational frequencies were representative of successful loading of HER and FA on synthesized AgNP surface.[28]

X-ray diffraction analysis of synthesized plasmonic nanoparticles

The structural features of synthesized HER-FA-AgNPs were explored with XRD by comparing its spectral pattern with that of the pure ingredients as shown in Figure 1e(i). HER-FA-AgNP exhibited [Figure 1e(ii)] specific diffraction peaks of AgNPs at 38.11° (111), 44.22° (200), 64.42°(220) and 77.48° (311) similar to previously reported studies.[29] However only few characteristic diffraction peaks observed in the XRD spectrum of raw ingredients or their physical mixture that mainly exist at 2θ between 20° to 30° (for HER: 27.71°, 25.52°, 28.81°, 29.93° and for FA: 27.10°, 29.40° and 22.75°)[30,31] were found in the spectral analysis of HER-FA-AgNPs which suggested the existence of HER and FA in amorphous condition in the NP formulation.[32] The surface modification or coating of NPs also contributed to generation of little noise and peak broadening as reported earlier.[33]

Hydrodynamic particle size and surface charge analysis along with morphological evaluation through transmission electron microscopy and EDX

Blank plasmonic AgNPs showed particle size of 27.83 ± 0.39 [Figure 2a] while HER-FA-AgNPs was of 50.25 ± 0.53 nm [Figure 2b] in size. HR-TEM in Figure 2e and f revealed the synthesized anisotropic nanocargoes to be distinctly pentagonal nanopyramids in shape. The PDI values of both AgNPs and HER-FA-AgNPs, 0.248 ± 0.04 and 0.274 ± 0.06, respectively, indicated the nanoparticles (PDI < 3) to be dispersed uniformly and homogeneously. On analysis, AgNPs revealed zeta potential of −23.8 mV [Figure 2c] which may occur as a result of using citrate as capping agent. HER-FA-AgNPs revealed a further negative surface charge of −32.7 mV [Figure 2d] that may be due to folic acid functional groups.[34]

On the other hand, the energy dispersive X-ray spectroscopy (EDAX) [Figure 2g] confirmed presence of elemental silver (Ag) in the synthesized nanoparticles as NPs with characteristic and prominent absorption peak near to 3KeV correspond to metallic silver designated SPR.[26,35] The crystallinity and diffraction peaks of HER-FA-AgNPs which was demonstrated in XRD to be indexed to (111), (200), (220) and (311) plane of face centered cubic crystal AgNP structure was confirmed by SAED [Figure 2h].[29,36]

Drug loading and stability studies of HER-FA-AgNPs

Loading efficiency of HER-FA-AgNPs was explored using UV-Vis spectrophotometer and theoretical DLC. At a set value of 10wt% of theoretical DLC, the drug loading capacity was determined to be 8.01% which implicated successful quenching of HER to surface of synthesized plasmonic AgNPs.

Stability being a primary requirement of any nano-formulation, alteration in terms of particle size and PDI of HER-FA-AgNPs were checked over a period of 14 days. The variations in hydro-dynamic diameter [Figure 3a(i)] as well as PDI [Figure 3a(ii)] of HER-FA-AgNPs were studied to be within the acceptable limit throughout the entire incubation period suggesting nano-formulation to be stable without

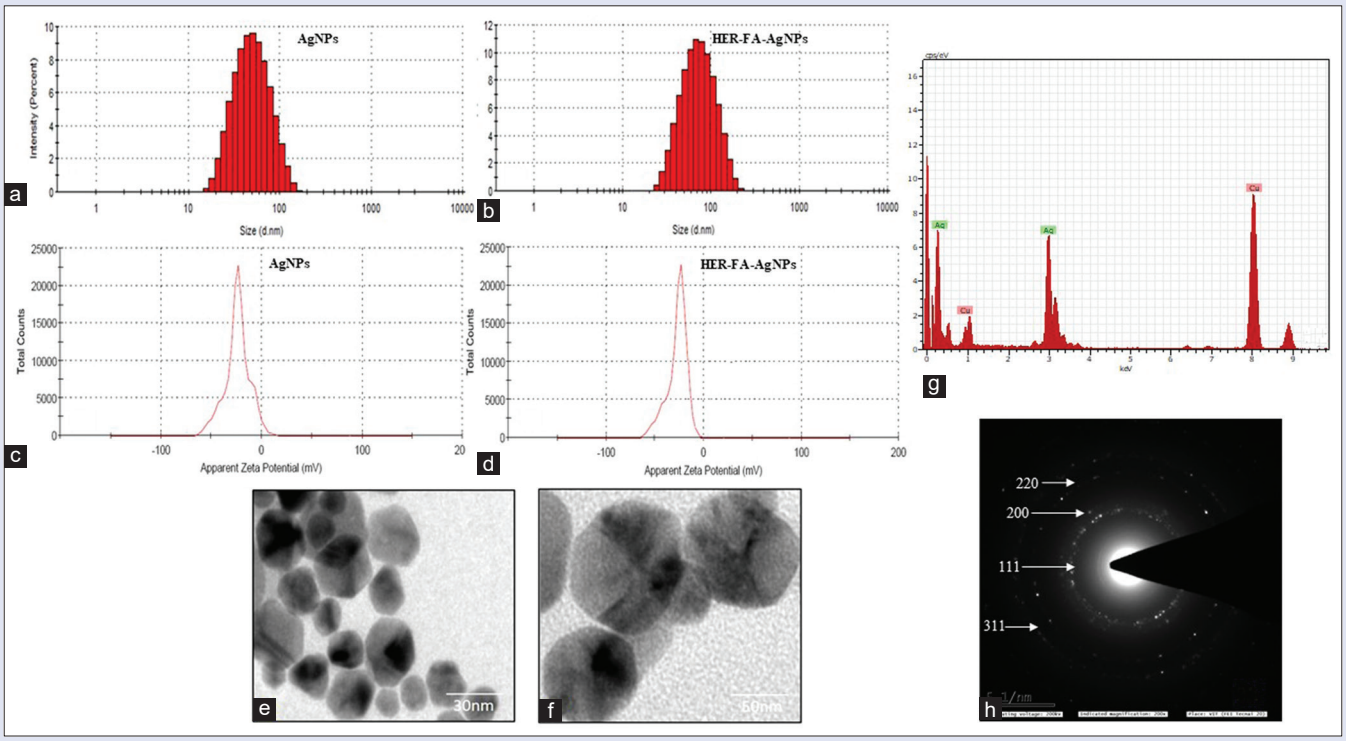

Figure 2: Morphological analysis of silver nanoparticles. Particle size distribution of (a) AgNPs and (b) HER-FA-AgNPs and zeta potential of (c) AgNPs and (d) HER-FA-AgNPs, High resolution transmission electron microscopy images of (e) AgNPs and (f) HER-FA-AgNPs, (g) EDAX of HER-FA-AgNPs (h) SAED analysis of HER-FA-AgNPs; HER: Herniarin, FA: Folic acid, FA-AgNPs: Folic acid fabricated silver nanoparticles, HER-FA-AgNPs: HER quenched folic acid modified silver nanoparticles, AgNPs: Silver nanoparticles, EDAX: Energy dispersive X-ray spectroscopy, SAED: Selective area electron diffraction

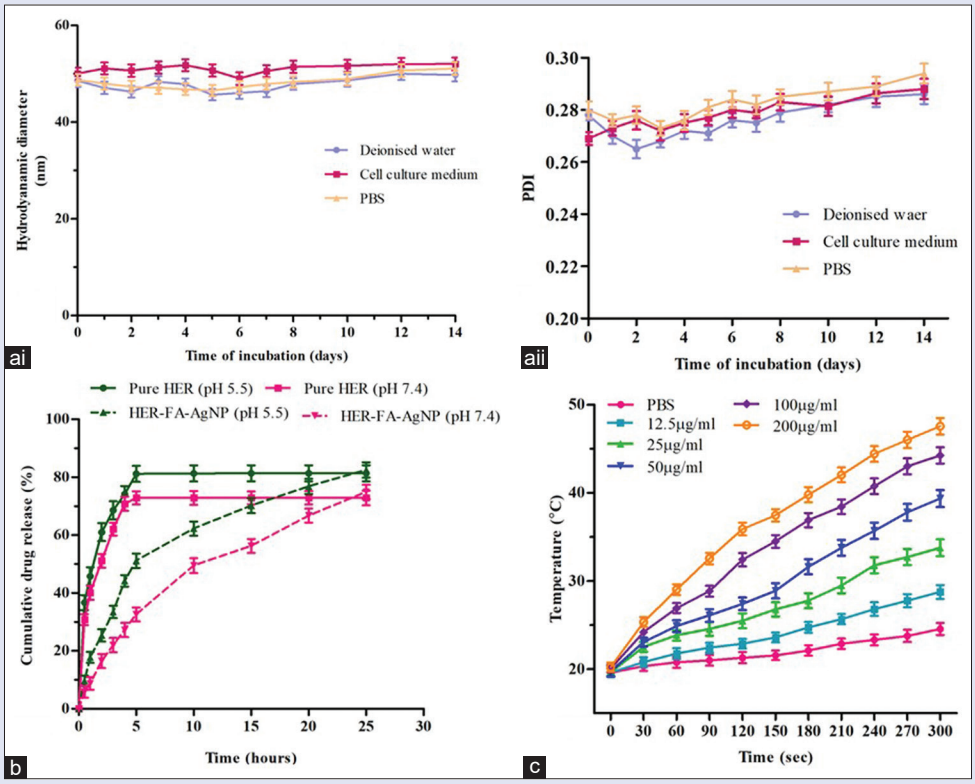

Figure 3: (a) Chemical stability of the synthesized HER-FA-AgNPs in 3 biologically relevant medium (deionized water, cell culture medium, PBS) with respect to (i) hydrodynamic diameter and (ii) PDI, (b) The cumulative release study of HER (pure) at pH 5.5 and 7.4, respectively, and HER-FA-AgNPs at pH 5.5 and 7.4, (c) evaluation of thermal profiles of PBS and different concentrations (12.5, 25, 50, 100 and 200 µg/ml) of HER-FA-AgNPs under exposure to 5 min of NIR laser irradiation; HER: Herniarin, FA: Folic acid, FA-AgNPs: Folic acid fabricated silver nanoparticles, HER-FA-AgNPs: Herniarin quenched folic acid modified silver nanoparticles, AgNPs: Silver nanoparticles, NIR: Near infrared

particle aggregation in all the three biologically relevant media of deionized water, cell culture medium and PBS.

Drug release study

Regulating the drug release pattern of HER-FA-AgNPs plays a key role in influencing the bioavailability of the HER. In the current study, cumulative percentage of HER released was analyzed in 2 buffered aqueous solutions (at 37°C) of pH 5.5 mimicking the tumor microenvironment or intracellular endosomes and pH physiological pH of 7.4 [Figure 3b]. The results indicated that the acidic pH facilitated release of HER than the neutral pH. In contrast to the free HER solution, that showed rapid release of drug accounting >81% over 5 h in pH 5.5, HER-FA-AgNPs governed the release of HER in a steady and sustained manner causing only 51% leakage over 5 h. The capability of archetypal delivery system to release adequate amount of drug preferably upto a longer duration of time determines its optimum therapeutic efficacy.[37] As evident from the release curve, although the released drug from raw HER solution reached saturation after 5 h, the synthesized nanocarriers efficiently leached >82% of the drug in a controlled fashion in the acidic pH over 25 h thus denoting the efficacy of the nanocarriers for enhanced HER release at tumor selective acidic pH.

HER-FA-AgNPs merit as potential photothermal agent

The ability of plasmonic HER-FA-AgNPs to promote photothermal effects was determined by tracking variation in temperature upon laser irradiation. As illustrated in Figure 3c, in comparison to PBS the temperature of HER-FA-AgNP solution was found to increase gradually in concentration dependent fashion. The temperature monitored for HER-FA-AgNPs at 200 µg/ml was markedly raised to 47.55°C upon NIR exposure for 5 min. This result indicated successful resonance of the electromagnetic field of laser beam with NP's plasmonic field that finally results in dissipation of absorbed energy in form of heat thereby increasing the temperature of NP solution.

Cytotoxicity of HER-FA-AgNPs

MTT assay was performed to evaluate the cytotoxic effect of the synthesized NPs. As shown in Figure 4, gradual and dose dependent augmentation of toxicity was exhibited by AgNPs, HER, HER-AgNPs, HER-FA-AgNPs and HER-FA-AgNPs+NIR treatment at different concentrations of drugs ranging from 12.5 to 200 µg/ml for 48 h. The IC_{50} value of HER-FA-AgNPs was found to be 11.86 µg/ml [Figure 4b(iv)] and indicated significant inhibitory potential on MDA-MB-231 cells ($n = 3$). Concurrently when exposed to NIR irradiation (800 nm, 1.5Wcm^{-2}, 5 min), in combination with HER-FA-AgNPs the viability of cells was found to diminish further. As evident from the results, FA functionalized NPs facilitated targeted drug delivery to the cancer cells through the overexpressed FRs while hyperthermia caused by laser exposure spontaneously improved the cytotoxicity in breast cancer cells.

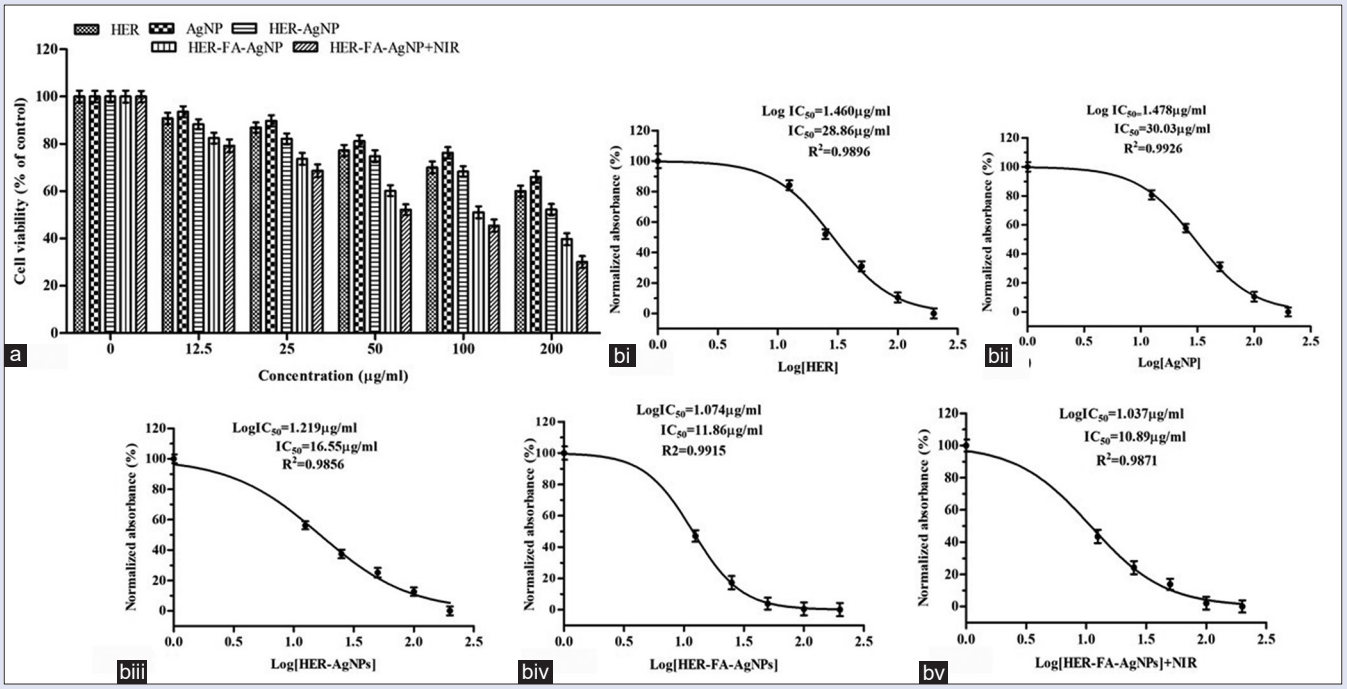

Figure 4: (a) Cell cytotoxicity analysis through MTT using MDA-MB-231 breast cancer cells followed by 48 h treatment with various concentration (12.5, 25, 50, 100 and 200 µg/ml) of raw HER, blank AgNP, HER-AgNP, HER-FA-AgNP and HER-FA-AgNP + NIR ($n = 3$); (b) IC_{50} value analysis, HER: Herniarin, FA: Folic acid, HER-AgNPs: HER quenched silver nanoparticles, HER-FA-AgNPs: Herniarin quenched folic acid modified silver nanoparticles, AgNPs: Silver nanoparticles, NIR: Near infrared

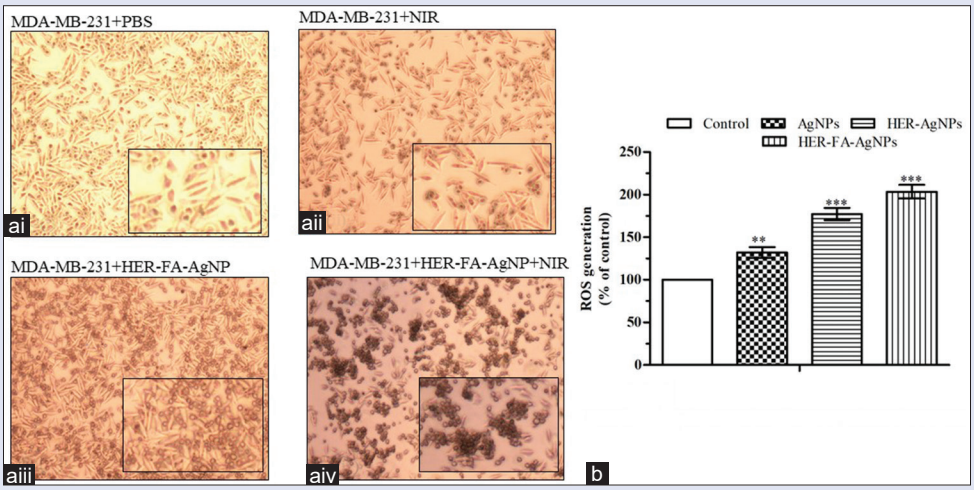

Figure 5: (a) Potential of HER-FA-AgNPs to induce hyperthermia mediated cytotoxicity and morphological transfiguration in MDA-MB-231 observed by contrast (light) phase microscopy after treating with only NIR, HER-FA-AgNPs and HER-FA-AgNPs + NIR, (b) Quantification of intracellular ROS production in MDA-MB-231 cell line ($n = 3$) following treatment with AgNP, HER-AgNP and HER-FA-AgNP; where $^{***}P < 0.001$; $^{**}P < 0.01$; $^{*}P < 0.05$; $^{ns}P > 0.05$ versus control, HER: Herniarin, FA: Folic acid, HER-FA-AgNPs: Herniarin quenched folic acid modified silver nanoparticles, AgNPs: Silver nanoparticles, ROS: Reactive oxygen species, NIR: Near infrared

The chemo-photothermal ablation by HER-FA-AgNPs transmuted cellular morphology of MDA-MB-231 cells

As depicted in Figure 5a, in absence of any treatment, MDA-MB-231 cells demonstrated characteristics of epithelial (smooth) cells possessing distinct nuclei [Figure 5a(i)]. In contrast, HER-FA-AgNPs treated BC cells [Figure 5a(iii)] represented distinguished morphological anomalies as they were found to lack cell to cell connection along with attainment of cell rounding. Upon laser irradiation, the cells treated with HER-FA-AgNPs further exhibited [Figure 5a(iv)] aggravated clustering together with simultaneous indications of cell-shrinkage, chromatin condensation and cell surface blebbing typical of apoptosis that suggest that hyperthermia in combination with chemotherapeutic efficacy begat by HER-FA-AgNP accentuated its cytotoxic potential. These prominent structural modifications further directed our study to

explore the chemo-photothermal efficacy of these NPs in *in-vivo* BC model.

HER-FA-AgNPS facilitated reactive oxygen species generation in MDA-MB-231 cell lines

The capability of different synthesized nano-formulations to induce ROS production was estimated by DCFH-FA technique. Figure 5b depicts the efficacy of HER-AgNPs and HER-FA-AgNPs ($P < 0.001$) to provoke prominent ROS accumulation in MDA-MB-231 cells.

Restorative potential of HER-FA-AgNPs on cancer induced tumor and body weight

As shown in Figure 6b there was exponential growth in tumor volume ($P < 0.001$) in group II animals following tumor induction. In contrast to the free HER and blank AgNPs treated experimental groups, the HER nanocarriers showed significant ($P < 0.001$) reduction in tumor volume in comparison to group II animals. But when functionalized with FA, owing to improved and targeted tumor site accumulation, HER-FA-AgNPs remarkably ameliorated the tumor volume ($P < 0.001$) in group VI animals. The animals in group VII that received HER-FA-AgNPs (i.v.) followed by irradiation of tumor region by 800 nm laser showed a further decline in tumor volume ($P < 0.001$) that may be due to the combined effect of active targeting, chemotherapy and photo thermal ablative effects of HER-FA-AgNPs.

Correlating with the efficiency of HER-FA-AgNPs in shrinking the tumor volume, simultaneous positive effects were observed on the body weight of breast tumor bearing animals that reinstated the body weight alterations. Both groups (VI and VII) of animals receiving, respectively, HER-FA-AgNPs and NIR laser therapy following NPs administration significantly improved the body weight ($P < 0.001$) in comparison to DMBA induced SD rats in group II. Based on active FR-targeting, HER quenched FA-AgNPs significantly restored the b.w. almost back to normalcy in group VI animlas showing mere difference ($P < 0.01$) with control animals (group I) while combined laser mediated hyperthermia with chemotherapeutic potential of HER-FA-AgNPs in group VII showed maximum potential ($P > 0.05$) resulting in insignificant difference with group I animals.

HER-FA-AgNPs mediated combined chemo-photothermal therapy reinstated the typical cellular architecture in DMBA induced rats

The *in-vivo* antitumor efficacy of the synthesized plasmonic nano-formulation was further investigated at tissue levels with histopathological analysis [Figure 7a]. The breast tissues isolated from control (group I) animals manifested [Figure 7a(i)] resting profile with normal parenchyma along with interstitial tissue comprising mainly fatty tissues and narrow connective tissue surrounded lobular units. Also, acini and ductules were observed to have normal forms. In contrast, group II animals revealed altered tumor morphology [Figure 7a(ii)] with disrupted mammary ducts associated with proliferating lumen that lead to ductal hyperplasia. Proliferative lesions were also evident with altered and enlarged lobular alveoles marked with cribriform arranged cells. Fused glandular structure characteristic of ductal carcinoma (adenocarcinoma) resulted from exhaustive epithelial proliferation. Epithelial ductal cells also appeared to be uniformly neoplastic, apparent with nuclear polymorphism associated with marked enlargement of nucleus, hyper-chromatinization, as well as chromatid clumping. On the other hand, animals in groups receiving HER [Figure 7a(iv)], HER-AgNPs [Figure 7a(v)] demonstrated moderate traces of improvement in the intratumor cellular anomalies. HER-FA-AgNPs intervention however exhibited substantial reversal of hyperplasia and abated abnormal proliferation along with initial signs of restoration of typical mammary ductal and alveolar structure. But the combined chemo-PTT [Figure 7a(vii)] revealed extraordinary efficacy in achieving cellular assassination thereby establishing uniformly arranged epithelial cells and lack of hyperplasia. Also, implication of apoptosis was also visible with the appearance of round, heavily stained apoptotic bodies representing fragmented nuclear parts.

HER-FA-AgNPs restored normal architecture during field emission scanning electron microscope analysis in breast cancer tissue

The morphological alterations in breast tissues were further evaluated by FESEM [Figure 8]. As exhibited by Figure 8a(i), cancer induced breast

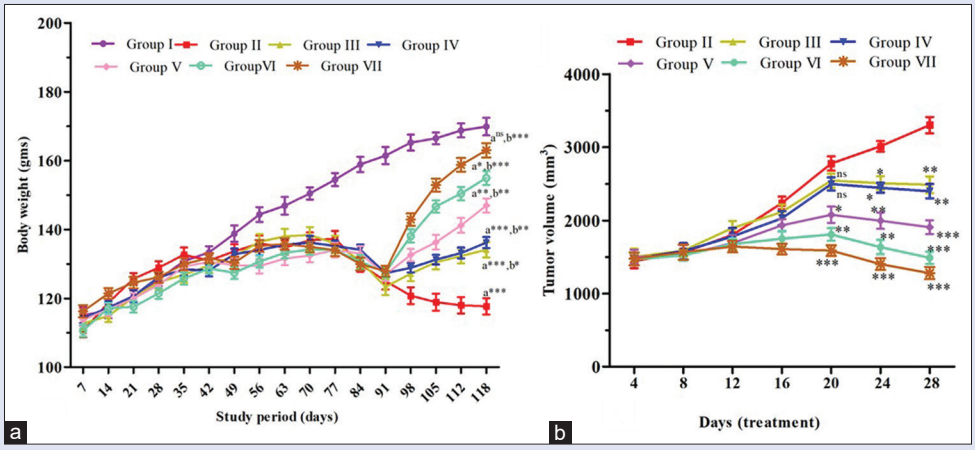

Figure 6: *In-vivo* analysis of efficacy of chemo-photothermal effect of HER-FA-AgNPs on (a) body weight (b) tumorigenesis assessment in cancer induced rats where each value shows mean ± standard error of the mean ($n = 6$); comparisons: a-Group II, III, IV, V, VI, VII compared with Group I; b-Group III, IV, V, VI, VII compared to Group II; ***$P < 0.001$; **$P < 0.01$; *$P < 0.05$; $^{ns}P > 0.05$; Group I-Control; Group II-Induced control (DMBA, 20 mg); Group III-DMBA (20 mg) +AgNP (40 mg/kg, b. w.); Group IV-DMBA (20 mg) + HER (20 mg/kg, b. w.); Group V-DMBA (20 mg) + HER-AgNP (20 mg/kg, b. w.); Group VI-DMBA (20 mg) + HER-FA-AgNP (20 mg/kg, b. w.), Group VII-DMBA (20 mg) + HER-FA-AgNP (20 mg/kg, b. w.) + c. w. NIR (800 nm, 1.5 Wcm^{-2}, 5 min); DMBA: 7,12-dimethylbenz (a) anthracene. HER: Herniarin, FA: Folic acid, FA-AgNPs: Folic acid fabricated silver nanoparticles, HER-FA-AgNPs: Herniarin quenched folic acid modified silver nanoparticles, AgNPs: Silver nanoparticles, NIR: Near infrared radiation

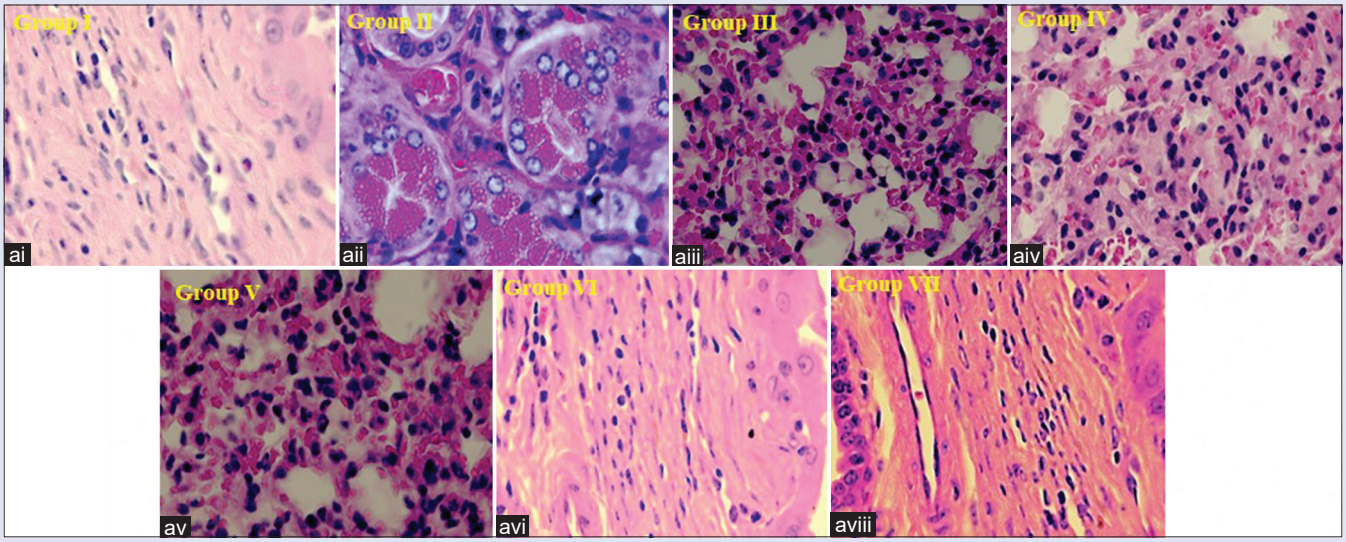

Figure 7: (a) Histopathological evaluation (×400) of breast tissues obtained from different groups of experimental animals, where a (i) Group I: Control, a (ii) Group II-Induced control (DMBA, 20 mg), a (iii) Group III-DMBA (20 mg) +AgNP (40 mg/kg, b. w.), a (iv) Group IV-DMBA (20 mg) + HER (20 mg/kg, b. w.), a (v) Group V-DMBA (20 mg) + HER-AgNP (20 mg/kg, b. w.), a (vi) Group VI-DMBA (20 mg) + HER-FA-AgNP (20 mg/kg, b. w.); a (vii) Group VII-DMBA (20 mg) + HER-FA-AgNP (20 mg/kg, b. w.) + c. w. NIR (800 nm, 1.5 Wcm^{-2}, 5 mins); DMBA: 7,12-dimethylbenz (a) anthracene, HER: Herniarin, FA: Folic acid, HER-AgNPs: HER quenched silver nanoparticles, HER-FA-AgNPs: Herniarin quenched folic acid modified silver nanoparticles, AgNPs: Silver nanoparticles, NIR: Near infrared radiation

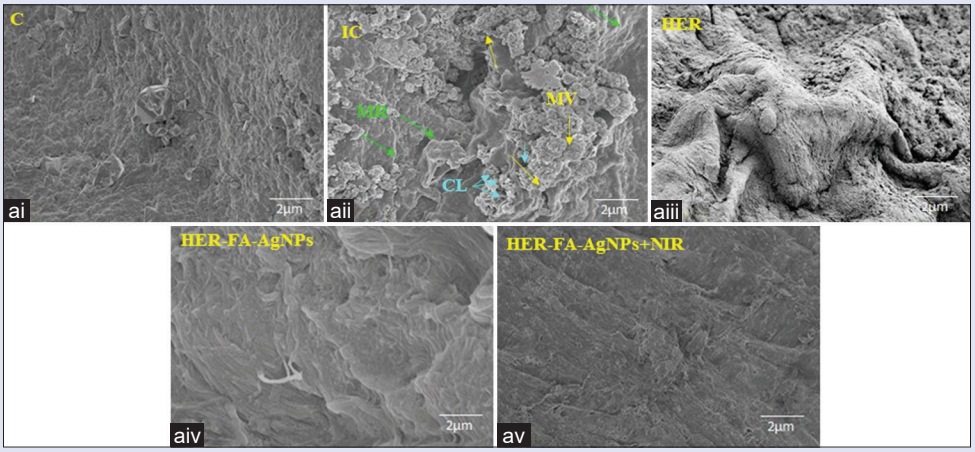

Figure 8: FESEM analysis of breast tumor tissue isolated from different experimental groups of animals to evaluate the structural modifications at tissue level where a (i) C: Control (group I), a (ii) IC: Induced control (Group II), a (iii) HER: DMBA (20 mg) + HER (20 mg/kg, b. w.) treated group (group IV), a (iv) HER-FA-AgNPs: DMBA (20 mg) + HER-FA-AgNP (20 mg/kg, b. w.) treated group (group VI) and a (v) HER-FA-AgNPs + NIR: DMBA (20 mg) + HER-FA-AgNP (20 mg/kg, b. w.) + laser (c. w. NIR 800 nm, 1.5 Wcm^{-2}, 5 mins) treated group (group VII); DMBA: 7,12-dimethylbenz (a) anthracene, HER: Herniarin, FA: Folic acid, HER-FA-AgNPs: Herniarin quenched folic acid modified silver nanoparticles, AgNPs: Silver nanoparticles, NIR: Near infrared radiation

tissue showed membrane ruffles (MR) that indicates the invasiveness of breast cancer and was found to be densely covered with microvilli (MV). Also, collagen fibres originating in surrounding matrix were observed to crosslink and form network. However, after treatment MR and MV were markedly reduced [Figure 8a(iv)] while prominent reduction in collagen fibre network was also visible and almost disappeared after irradiation to NIR subsequent to HER-FA-AgNP treatment [Figure 8a(v)]. Thus, the efficacy of chemo-photothermal treatment was once again evident in restoring normal architecture of the breast tissue.

DISCUSSION

Breast cancer is a debilitating malignancy that has emerged as a global terror with TNBC being the most aggressive malignant neoplasm.[38] Conventional chemotherapy or single mode approach with apparent drawbacks of limited selectivity, extensive off-target side effects and increasing resistance for BC cells including TNBC[39,40] merit multi-modal combination pharmacotherapeutic as a future approach as a future strategy to conquer cancer. The recent advancements in the field of phytotherapy and nanotechnology[41] envisage natural bioactive moiety quenched pleotropic AgNPs as a promising, safe and specific therapeutic option for BC. Thus, the current study explored the efficacy of novel plasmonic HER-FA-AgNPs to induce chemo-photothermal treatment in BC.

Different factors like synthesis route, particle size, shape, stability, drug loading etc., are some of the crucial parameters that need to be properly judged for the optimal design and synthesis of AgNPs. It is

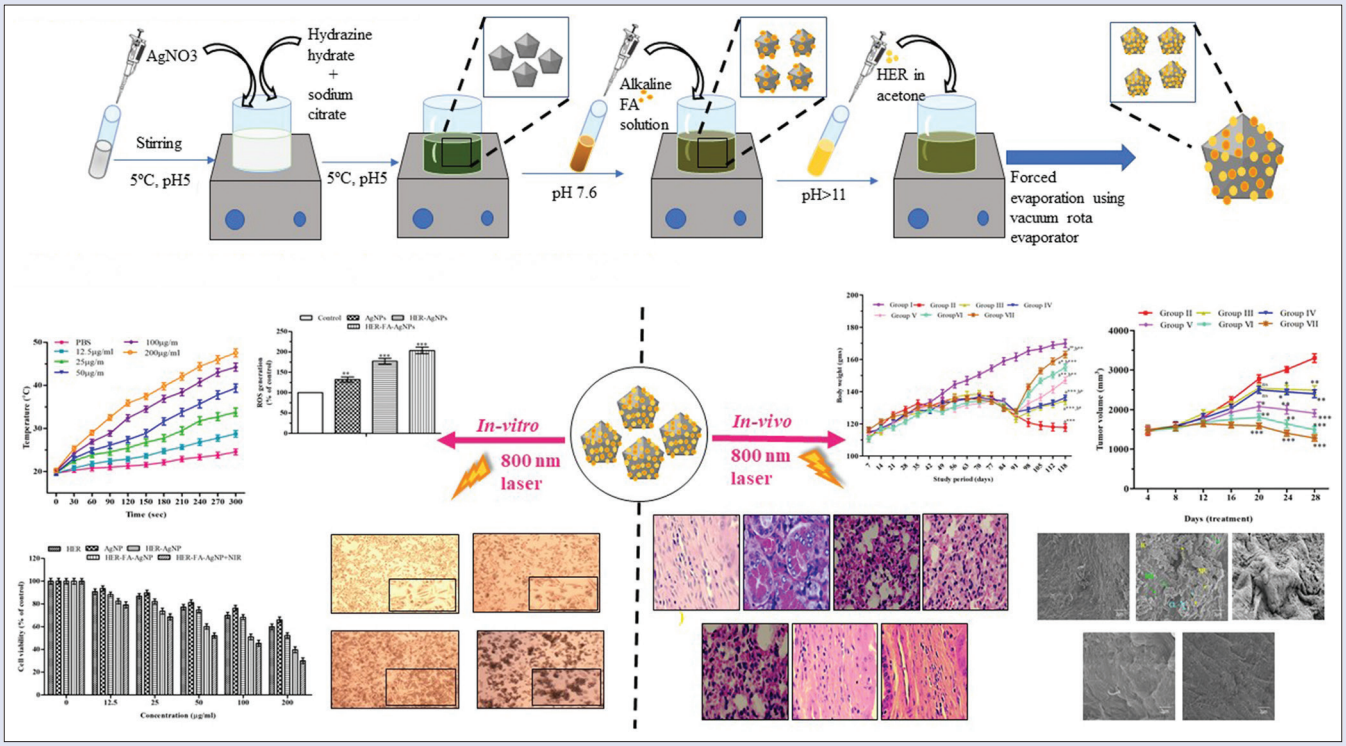

Figure 9: The synthesis protocol of HER-FA-AgNPs and its efficacy in *in-vitro* (MDA-MB-231) breast cancer cell line and *in-vivo* in DMBA induced breast cancer model in Sprague Dawley rats (pictorial abstract)

well known that NPs' distribution throughout the body depends on the particle size since larger particle size results in faster clearance in blood and distribution in spleen, liver and lungs. NPs in range of 10–200 nm possessing negatively charged surface are observed to have slower clearance rate from blood with better tendency of tumor accumulation.[42] From both DLS and TEM results it was evident that HER-FA-AgNPs were well below 100 nm that contributed for feasible cellular entry. In case of plasmonic NPs, the shape plays a pivotal role. Interaction of AgNPs with electromagnetic radiation (e.g., photons) confers in a strong localized SPR.[43,44] However conventional spherical AgNPs generate plasmonic resonance that are typically restricted in the visible spectrum range (400 nm–500 nm)[45] that limits their application in biological tissue owing to absorption of visible tissue-mediated light.[46] With the highest plasmonic excitation capacity among gold, silver and copper,[47] efficient plasmon peak tunability can be achieved by altering the size and shape of silver-based nano-formulations. Anisotropic nanocrystals based on their robust plasmonic characteristics in biological window (650–1200 nm) becomes ideally suitable for various biomedical application including PTT.[48] As reported previously, harnessing stabilizer-reductant hydrogen bond interaction acts as a crucial parameter for anisotropic growth of nanoparticles,[20] we also followed a simple one pot synthesis method for preparing anisotropic plasmonic AgNPs,[20] which were later quenched by a novel method with FA and HER. As revealed from our HR-TEM results, the near IR plasmonic NPs were pentagonal nanopyramids with efficient tunable UV-Vis-NIR plasmon peaks facilitating light absorption at higher (817 nm) wavelength thus enabling deep tissue penetration which correlated with earlier studies documenting similar phenomenon due to plasmon coupling among adjoining NPs.[49] As illustrated from our UV spectroscopy results, the AgNPs, following surface modification by FA and HER showed marked red shift of the plasmon peaks that validated their physical association with AgNPs.[50,51] Nanoparticles with negative surface charge is reported with diminished plasma-protein adsorption and truncated rate of indefinite cellular uptake.[42,52] Thus HER-FA-AgNPs possessing-32.7 zeta potential successfully overcame natural aggregation tendency by repelling one another that allowed stable blood dispersion and favorable tumor tissue accumulation owing to EPR effect.[53] Moreover, as denoted by the stability studies, limited variations in particle size and PDI confirmed HER-FA-AgNPs to be stable that characterize NPs behavior in blood stream.[54] Similarly, as environment responsive degradation of AgNPs with pathological site-specific drug release (i.e., high efflux at corresponding acidic pH) attracts attention,[55] sufficient drug release from HER-FA-AgNPs validates it as effective carrier system for drug delivery in acidic tumor microenvironment[26] thereby providing consolidated creative output.[56] Apart from all these parameters, AgNPs also corresponded to other typical earlier reported physico-chemical features in terms of XRD, EDAX and SAED.

AgNPs have been reported to exhibit cytotoxic potential against widespread cancer types including breast, ovary, brain, cervix, liver, colon, lungs, pancreas and blood.[37] Several studies have reported the AgNPs as prospective carrier system for miscellaneous well-known anti-cancer drugs including doxorubicin,[57] methotrexate,[32] imatinib,[56] as well as potent phytoconstituents like berberine,[36] curcumin[58] etc. On the other hand, receptor based active drug targeting of nano cargoes has been widely researched in which FA functionalized NPs have manifested diversified therapeutic and imaging applications.[34] Overexpressed FRs in breast cancer, specifically in TNBC patients, usually correlated with decreased survival, thus contributes in significant enhancement of targeted uptake of FA navigated AgNPs.[59] On the other hand, HER is known to have therapeutic effect in breast cancer. Since, anticancer agents and NPs as combination therapy influence synergistic effect and causes plausible suppression of drug resistance, we also evaluated the efficacy of HER-FA-AgNPs through different *in-vitro* and *in-vivo* studies. As revealed by MTT assay, although raw HER caused inhibitory effect on viability of FR (+ve) MDA-MB-231 (TNBC) cells,[60] but the cytotoxic potential was

many folds higher in case of HER-FA-AgNPs which showed its efficacy in dose dependent fashion. This increased rate of inhibiting cell viability may be the consequence of FR-targeted drug delivery system that resulted in site specific action in similar ways to other researches.[34,36] Also, in corollary to previous findings indicating production of ROS by AgNPs as one of their cytotoxic mechanism to induce apoptosis, HER-FA-AgNPs were also observed to induce oxidative stress in breast cancer cell lines. This enhanced ROS is usually generated due to the tendency of AgNPs for mitochondrial localization leading to its damage.[61]

The unique optical features of AgNPs are being recently exploited to investigate new prospects in the field of light activated therapeutics. Plasmonic NPs ensuing tumor localization enact as novel photothermal transducers by transforming the absorbed light by surface plasmonic resonance into heat thereby conferring in therapeutic killing of cells due to localized temperature elevation.[62] Thus, plasmonic AgNPs triggered hyperthermia serves as a new paradigm for allied cancer treatment at cellular as well as sub-cellular level.[63] Several studies have already reported the efficacy of PTT in controlling and treating tumor cells mediated by AgNPs. Phase contrast microscopy revealed extraordinary results of its maximum inhibitory effect on MDA-MB-231 cytotoxicity when irradiated with NIR laser.[64,65] This finding indicated the efficacy of HER-FA-AgNPs to incite *in-vitro* hyperthermia thereby resulting in an advanced chemo-photo thermal activity which can drastically improve the BC treatment. Identical observations were reported earlier in different (liver, lungs, ovarian etc.) cancer cells including breast cancer.[34,51,66,67]

Our *in-vivo* studies in DMBA induced breast cancer bearing rats evinced results that reflected and revalidated the *in-vitro* effects of HER-FA-AgNPs. Owing to the combined chemo-photothermal effect, cancer induced altered body weight of animals receiving HER-FA-AgNPs with subsequent NIR irradiation were reinstated almost back to normalcy while their tumor burden was also significantly minimized.[36] Thus, the combined effect of chemotherapy and hyperthermia provoked by HER-FA-AgNPs upon exposure to NIR laser signified most prominent protective effects against BC. Also, histomorphological investigations demonstrated HER-FA-AgNPs accompanied by NIR laser to be most proficient in restoring the normal breast tissue physiology as its chemo photothermal effect minimized atypical hyperplasticity and ductal canceration.[68]

CONCLUSION

The current findings suggest FR targeted HER quenched plasmonic AgNPs to be successful in achieving combined chemo-photo thermal anti-breast cancer therapy [Figure 9]. Not only did the formulated NPs surmount the hydrophobic nature of HER but allowed its target release at tumor specific site to potentiate the antitumor effect of HER. Moreover, hyperthermia mediated cancer cells assassination by HER-FA-AgNPs augmented its chemotherapeutic potency. Overall, such multimodal novel NPs may pose to be beneficial for improving the available therapeutic options for BC.

Acknowledgements

The authors are immensely thankful to the BIT and Central Instrumentation facility (CIF) for offering all the necessary facilities and infrastructure for uninterrupted conduct of this work. Also, we are grateful for the contribution of VIT instrumentation facility for conduction TEM of the nanoparticles.

Financial support and sponsorship

This research was fully funded by AICTE under the project Grant No. 8-69/RIFD/RPS/POLICY-1/2016-17.

Conflicts of interest

There are no conflicts of interest.

REFERENCES

1. Cinkaya A, Akin M, Sengul A. Evaluation of treatment outcomes of triple-negative breast cancer. J Cancer Res Ther 2016;12:150-4.
2. Kapadia GJ, Rao GS, Ramachandran C, Iida A, Suzuki N, Tokuda H. Synergistic cytotoxicity of red beetroot (*Beta vulgaris L.*) extract with doxorubicin in human pancreatic, breast and prostate cancer cell lines. J Complement Integr Med 2013;10:1-10.
3. Kim TH, Shin YJ, Won AJ, Lee BM, Choi WS, Jung JH, *et al.* Resveratrol enhances chemosensitivity of doxorubicin in multidrug-resistant human breast cancer cells via increased cellular influx of doxorubicin. Biochim Biophys Acta 2014;1840:615-25.
4. Harvey RG, Cortez C, Ananthanarayan TP, Schmolka S. A new coumarin synthesis and its utilization for the synthesis of polycyclic coumarin compounds with anticarcinogenic properties. J Org Chem 1988;53:3936-43.
5. Payá M, Halliwell B, Hoult JR. Interactions of a series of coumarins with reactive oxygen species. Scavenging of superoxide, hypochlorous acid and hydroxyl radicals. Biochem Pharmacol 1992;44:205-14.
6. Fylaktakidou KC, Hadjipavlou-Litina DJ, Litinas KE, Nicolaides DN. Natural and synthetic coumarin derivatives with anti-inflammatory/antioxidant activities. Curr Pharm Des 2004;10:3813-33.
7. Mousavi SH, Davari AS, Iranshahi M, Sabouri-Rad S, Tayarani Najaran Z. Comparative analysis of the cytotoxic effect of 7-prenyloxycoumarin compounds and herniarin on MCF-7 cell line. Avicenna J Phytomed 2015;5:520-30.
8. Kielbus M, Skalicka-Wozniak K, Grabarska A, Jeleniewicz W, Dmoszynska-Graniczka M, Marston A, *et al.* 7-substituted coumarins inhibit proliferation and migration of laryngeal cancer cells *in vitro*. Anticancer Res 2013;33:4347-56.
9. Bose P, Pattanayak SP, Herniarin, a natural coumarin, inhibits mammary carcinogenesis by modulating liver X receptor-α/β-PI3K-Akt-Maf1 Pathway in sprague-dawley rats. Pharmacog Mag 2019;15:510.
10. Gromadzki D, Tzankova V, Kondeva M, Gorinova C, Rychter P, Libera M, *et al.* Amphiphilic core-shell nanoparticles with dimer fatty acid-based aliphatic polyester core and zwitterionic poly (sulfobetaine) shell for controlled delivery of curcumin. Int J Polym Mater PO 2017;66:915-25.
11. Cheng W, Nie J, Xu L, Liang C, Peng Y, Liu G, *et al.* pH-sensitive delivery vehicle based on folic acid-conjugated polydopamine-modified mesoporous silica nanoparticles for targeted cancer therapy. ACS Appl Mater Interfaces 2017;9:18462-73.
12. Austin LA, Mackey MA, Dreaden EC, El-Sayed MA. The optical, photothermal, and facile surface chemical properties of gold and silver nanoparticles in biodiagnostics, therapy, and drug delivery. Arch Toxicol 2014;88:1391-417.
13. Chairuangkitti P, Lawanprasert S, Roytrakul S, Aueviriyavit S, Phummiratch D, Kulthong K, *et al.* Silver nanoparticles induce toxicity in A549 cells via ROS-dependent and ROS-independent pathways. Toxicol *In vitro* 2013;27:330-8.
14. Kittler S, Greulich C, Diendorf J, Koller M, Epple M. Toxicity of silver nanoparticles increases during storage because of slow dissolution under release of silver ions. Chem Mater 2010;22:4548-5454.
15. Huang X, Jain PK, El-Sayed IH, El-Sayed MA. Plasmonic photothermal therapy (PPTT) using gold nanoparticles. Lasers Med Sci 2008;23:217-28.
16. Jaque D, Martínez Maestro L, del Rosal B, Haro-Gonzalez P, Benayas A, Plaza JL, *et al.* Nanoparticles for photothermal therapies. Nanoscale 2014;6:9494-530.
17. van der Zee J. Heating the patient: A promising approach? Ann Oncol 2002;13:1173-84.
18. Yang K, Zhang S, Zhang G, Sun X, Lee ST, Liu Z. Graphene in mice: Ultrahigh *in vivo* tumor uptake and efficient photothermal therapy. Nano Lett 2010;10:3318-23.
19. Chen Q, Liu X, Zeng J, Cheng Z, Liu Z. Albumin-NIR dye self-assembled nanoparticles for photoacoustic pH imaging and pH-responsive photothermal therapy effective for large tumors. Biomaterials 2016;98:23-30.
20. Pattanayak S, Swarnkar A, Priyam A, Bhalerao GM. Citrate-hydrazine hydrogen-bonding driven single-step synthesis of tunable near-IR plasmonic, anisotropic silver nanocrystals: Implications for SERS spectroscopy of inorganic oxoanions. Dalton Trans 2014;43:11826-33.
21. Kumar A, Sunita P, Jha S, Pattanayak SP. Daphnetin inhibits TNF-α and VEGF-induced angiogenesis through inhibition of the IKK s/IκBα/NF-κB, Src/FAK/ERK ½ and Akt signalling pathways. Clin Exp Pharmacol P 2016;43:939-50.

22. Ouhtit A, Gaur RL, Abdraboh M, Ireland SK, Rao PN, Raj SG, *et al.* Simultaneous inhibition of cell-cycle, proliferation, survival, metastatic pathways and induction of apoptosis in breast cancer cells by a phytochemical super-cocktail: Genes that underpin its mode of action. J Cancer 2013;4:703-15.
23. Niazvand F, Orazizadeh M, Khorsandi L, Abbaspour M, Mansouri E, Khodadadi A. Effects of quercetin-loaded nanoparticles on MCF-7 human breast cancer cells. Medicina (Kaunas) 2019;55:1-15.
24. Haque MW, Bose P, Siddique MU, Sunita P, Lapenna A, Pattanayak SP. Taxifolin binds with LXR (α & β) to attenuate DMBA-induced mammary carcinogenesis through mTOR/Maf-1/PTEN pathway. Biomed Pharmacother 2018;105:27-36.
25. Bose P, Siddique MU, Acharya R, Jayaprakash V, Sinha BN, Lapenna A, *et al.* Quinazolinone derivative BNUA-3 ameliorated [NDEA+2-AAF]-induced liver carcinogenesis in SD rats by modulating AhR-CYP1B1-Nrf2-Keap1 pathway. Clin Exp Pharmacol P 2020;47:143-57.
26. Balakrishnan S, Mukherjee S, Das S, Bhat FA, Raja Singh P, Patra CR, *et al.* Gold nanoparticles-conjugated quercetin induces apoptosis via inhibition of EGFR/PI3K/Akt–mediated pathway in breast cancer cell lines (MCF-7 and MDA-MB-231). Cell Biochem Funct 2017;35:217-31.
27. Ahmad A, Misra LN. Isolation of herniarin and other constituents from Matricaria chamomilla flowers. Int J Pharmacogn 1997;35:121-5.
28. Jeevitha D, Kanchana A. Evaluation of chitosan/poly (lactic acid) nanoparticles for the delivery of piceatannol, an anti-cancer drug by ionic gelation method. Int J Chem Environ Biolog Sci 2014;2:6.
29. Dadhich BK, Bhushan B, Saha A, Priyam A. Folate-directed shape-transformative synthesis of hollow silver nanocubes: Plasmon tunability, growth kinetics and catalytic applications. ACS Appl Nano Mater 2018;1:4294-305.
30. Umashankar T, Govindappa M, Ramachandra YL, Padmalatha Rai S. Channabasava. Isolation and characterization of coumarin isolated from endophyte, alternaria species-1 of Crotalaria pallida and its apoptotic action on HeLa cancer cell line. Metabolomics 2015;5:2153-0769.
31. Vora A, Riga A, Dollimore D, Alexander KS. Thermal stability of folic acid. Thermochim Acta 2002;392:209-20.
32. Thapa RK, Kim JH, Jeong JH, Shin BS, Choi HG, Yong CS, *et al.* Silver nanoparticle-embedded graphene oxide-methotrexate for targeted cancer treatment. Colloids Surf B Biointerfaces 2017;153:95-103.
33. Javed KR, Ahmad M, Ali S, Butt MZ, Nafees M, Butt AR, *et al.* Comparison of doxorubicin anticancer drug loading on different metal oxide nanoparticles. Medicine (Baltimore) 2015;94:e617.
34. Boca-Farcau S, Potara M, Simon T, Juhem A, Baldeck P, Astilean S. Folic acid-conjugated, SERS-labeled silver nanotriangles for multimodal detection and targeted photothermal treatment on human ovarian cancer cells. Mol Pharm 2014;11:391-9.
35. Nisar M, Khan SA, Qayum M, Khan A, Farooq U, Jaafar HZ, *et al.* Robust synthesis of ciprofloxacin-capped metallic nanoparticles and their urease inhibitory assay. Molecules 2016;21:411.
36. Bhanumathi R, Manivannan M, Thangaraj R, Kannan S. Drug-carrying capacity and anticancer effect of the folic acid- and berberine-loaded silver nanomaterial to regulate the AKT-ERK pathway in breast cancer. ACS Omega 2018;3:8317-28.
37. Zhang CZ, Niu J, Chong YS, Huang YF, Chu Y, Xie SY, *et al.* Porous microspheres as promising vehicles for the topical delivery of poorly soluble asiaticoside accelerate wound healing and inhibit scar formation *in vitro in vivo*. Eur J Pharm Biopharm 2016;109:1-3.
38. Fan W, Yung B, Huang P, Chen X. Nanotechnology for multimodal synergistic cancer therapy. Chem Rev 2017;117:13566-638.
39. Morton LM, Dores GM, Schonfeld SJ, Linet MS, Sigel BS, Lam CJK, *et al.* Association of chemotherapy for solid tumors with development of therapy-related myelodysplastic syndrome or acute myeloid leukemia in the modern era. JAMA Oncol 2019;5:318-25.
40. Mustacchi G, De Laurentiis M. The role of taxanes in triplenegative breast cancer: Literature review. Drug Des Dev Ther 2015;9:4303-18.
41. Hu A, Guo JY, Alarifi H, Patane G, Zhou Y, Compagnini G, *et al.* Low temperature sintering of Ag nanoparticles for flexible electronics packaging. App Phys Lett 2010;97:153117.
42. He C, Hu Y, Yin L, Tang C, Yin C. Effects of particle size and surface charge on cellular uptake and biodistribution of polymeric nanoparticles. Biomaterials 2010;31:3657-66.
43. Hutter E, Fendler JH. Exploitation of localized surface plasmon resonance. Adv Mater 2004;16:1685-706.
44. Hecht B, Bielefeldt H, Novotny L, Inouye Y, Pohl DW. Local excitation, scattering, and interference of surface plasmons. Phys Rev Lett 1996;77:1889-92.
45. Amendola V, Bakr OM, Stellacci F. A study of the surface plasmon resonance of silver nanoparticles by the discrete dipole approximation method: Effect of shape, size, structure and assembly. Plasmonics 2010;5:85-97.
46. Jacques SL. Optical properties of biological tissues: A review. Phys Med Biol 2013;58:R37-61.
47. Evanoff DD Jr, Chumanov G. Synthesis and optical properties of silver nanoparticles and arrays. Chemphyschem 2005;6:1221-31.
48. Andrew JC, Jennifer LW. Functional nanoparticles for bioanalysis, nanomedicine and bioelectronic device. J Am Chem Soc 2012;2:37-54.
49. Srinivasan S, Bhardwaj V, Nagasetti A, Fernandez-Fernandez A, McGoron AJ. Multifunctional Surface-Enhanced Raman Spectroscopy-Detectable Silver Nanoparticles Combined Photodynamic Therapy and pH-Triggered Chemotherapy. J Biomed Nanotechnol 2016;12:2202-19.
50. Sau S, Agarwalla P, Mukherjee S, Bag I, Sreedhar B, Pal-Bhadra M, *et al.* Cancer cell-selective promoter recognition accompanies antitumor effect by glucocorticoid receptor-targeted gold nanoparticle. Nanoscale 2014;6:6745-54.
51. Wang Z, Chang Z, Lu M, Shao D, Yue J, Yang D, *et al.* Janus silver/silica nanoplatforms for light-activated liver cancer chemo/photothermal therapy. ACS Appl Mater Interfaces 2017;9:30306-17.
52. Alexis F, Pridgen E, Molnar LK, Farokhzad OC. Factors affecting the clearance and biodistribution of polymeric nanoparticles. Mol Pharm 2008;5:505-15.
53. Aggarwal P, Hall JB, McLeland CB, Dobrovolskaia MA, McNeil SE. Nanoparticle interaction with plasma proteins as it relates to particle biodistribution, biocompatibility and therapeutic efficacy. Adv Drug Deliv Rev 2009;61:428-37.
54. Yang C, Attia AB, Tan JP, Ke X, Gao S, Hedrick JL, *et al.* The role of non-covalent interactions in anticancer drug loading and kinetic stability of polymeric micelles. Biomaterials 2012;33:2971-9.
55. Torchilin VP. Micellar nanocarriers: Pharmaceutical perspectives. Pharm Res 2007;24:1-6.
56. Sadat Shandiz SA, Shafiee Ardestani M, Shahbazzadeh D, Assadi A, Ahangari Cohan R, Asgary V, *et al.* Novel imatinib-loaded silver nanoparticles for enhanced apoptosis of human breast cancer MCF-7 cells. Artif Cells Nanomed Biotechnol 2017;45:1-0.
57. Li C, Yang XQ, Zhang MZ, Song YY, Cheng K, An J, *et al. In vivo* imaging-guided nanoplatform for tumor targeting delivery and combined chemo-, gene- and photothermal therapy. Theranostics 2018;8:5662-75.
58. Loo CY, Young PM, Lee WH, Traini D, Cavaliere R, Whitchurch CB, *et al.* Combination therapy of curcumin and silver nanoparticles with enhanced anti-biofilm activity for treatment of endotracheal tube-associated infections. J Aerosol Med Pulm D 2014;64:2513-22.
59. Hilgenbrink AR, Low PS. Folate receptor-mediated drug targeting: From therapeutics to diagnostics. J Pharm Sci 2005;94:2135-46.
60. Zhang Z, Wang J, Tacha DE, Li P, Bremer RE, Chen H, *et al.* Folate receptor α associated with triple-negative breast cancer and poor prognosis. Arch Pathol Lab Med 2014;138:890-5.
61. Hussain SM, Hess KL, Gearhart JM, Geiss KT, Schlager JJ. *In vitro* toxicity of nanoparticles in BRL 3A rat liver cells. Toxicol *In vitro* 2005;19:975-83.
62. Zharov VP, Galitovsky V, Viegas M. Photothermal detection of local thermal effects during selective nanophotothermolysis. Appl Phys Lett 2003;83:4897-99.
63. O'Neal DP, Hirsch LR, Halas NJ, Payne JD, West JL. Photo-thermal tumor ablation in mice using near infrared-absorbing nanoparticles. Cancer Lett 2004;209:171-6.
64. Khan MS, Talib A, Pandey S, Bhaisare ML, Gedda G, Wu HF. Folic Acid navigated Silver Selenide nanoparticles for photo-thermal ablation of cancer cells. Colloids Surf B Biointerfaces 2017;159:564-70.
65. Liu B, Zhou J, Zhang B, Qu J. Synthesis of Ag@ Fe3O4 nanoparticles for photothermal treatment of ovarian cancer. J Nanomater 2019;2019:1-6.
66. Boca SC, Potara M, Gabudean AM, Juhem A, Baldeck PL, Astilean S. Chitosan-coated triangular silver nanoparticles as a novel class of biocompatible, highly effective photothermal transducers for *in vitro* cancer cell therapy. Cancer Lett 2011;311:131-40.
67. Zhang W, Guo Z, Huang D, Liu Z, Guo X, Zhong H. Synergistic effect of chemo-photothermal therapy using PEGylated graphene oxide. Biomaterials 2011;32:8555-61.
68. Bodduluru LN, Kasala ER, Barua CC, Karnam KC, Dahiya V, Ellutla M. Antiproliferative and antioxidant potential of hesperetin against benzo (a) pyrene-induced lung carcinogenesis in Swiss albino mice. Chem Biol Interact 2015;242:345-52.